applied sciences

MDPI

Article

Research on Measuring Industrial Carbon Dioxide Emissions by Mobile Differential Absorption Lidar

Jinliang Zang [1,2,3,†], Liang Wu [2,3,†], Wanglong Shi [2,3], Hongjun Wang [1], Menghui Wu [4] and Hong Lin [1,2,3,*]

[1] Division of Thermophysics Metrology, National Institute of Metrology (China), Beijing 100029, China; zangjl@nim.ac.cn (J.Z.)
[2] Zhengzhou Institute of Metrology, Zhengzhou 450001, China
[3] Technology Innovation Center of Carbon Metrology, State Administration for Market Regulation, Zhengzhou 450001, China
[4] Fujian Institute of Metrology, Fuzhou 350003, China
* Correspondence: linhong@nim.ac.cn
† These authors contributed equally to this work.

Abstract

Industrial activities represent the primary source of anthropogenic carbon dioxide (CO_2) emissions, and accurate monitoring of industrial CO_2 emissions is critical to mitigating greenhouse gas emissions. Due to the lack of quantifiable and direct measurement technologies, industrial CO_2 emissions are typically calculated based on fuel combustion consumption and emission factors. However, the calculation method is not applicable to the quantification of fugitive emissions of CO_2. This work demonstrates the capability of remotely measuring industrial CO_2 emissions by mobile Differential Absorption Lidar (DIAL) system. The two-dimensional concentration distributions of the CO_2 plume were remotely measured using DIAL system, and the CO_2 emission rate was obtained with wind field information. The DIAL measurements were cross-validated using in-stack CEMS data and emission-factor calculations. Results show that the relative deviations of CO_2 emission rates between DIAL and CEMS range from −5.83% to +2.57% across four tests, all within ±6%, and the coefficient of variation (CV) of 27 valid datasets is 7.24%. In contrast, the emission factor method yields consistently higher estimates, with relative deviations of +4.61% compared to DIAL measurements. Furthermore, the mobile DIAL system was deployed in three industrial scenarios with different emission intensities: a natural gas-fired industrial park, a photovoltaic glass manufacturing plant (low-emission steady-state), and a coal-fired power plant (high-emission dynamic), demonstrating its preliminary adaptability under different operating conditions. This study indicates the feasibility and potential reliability of the mobile DIAL system for high spatio-temporal resolution remote measurement of industrial CO_2 emissions.

Keywords: DIAL; carbon dioxide; industrial emissions

Check for updates

Academic Editor: Nir Krakauer

Received: 3 April 2026
Revised: 27 April 2026
Accepted: 30 April 2026
Published: 6 May 2026

Copyright: © 2026 by the authors. Licensee MDPI, Basel, Switzerland. This article is an open access article distributed under the terms and conditions of the Creative Commons Attribution (CC BY) license.

1. Introduction

According to the Intergovernmental Panel on Climate Change (IPCC) 6th Assessment Report, carbon dioxide (CO_2), as the primary greenhouse gas (GHG), is the dominant contributor to global climate change [1]. Industrial activities represent the major anthropogenic source of CO_2 emissions, featured with high emission intensity and complex spatiotemporal distribution. Therefore, accurate measurement and monitoring of industrial CO_2

emissions are urgently required to support greenhouse gas mitigation and progress toward the "Net zero" goals [2].

At present, reported industrial CO_2 emissions are generally calculated based on fuel combustion consumption and emission factors. However, calculation-based methods (e.g., the IPCC 2006 baseline method) are affected by factors such as fuel composition, combustion efficiency, and accurate emission factors. Such methods typically carry substantial uncertainties, with values commonly ranging from ±10% to ±30% [3,4]. Moreover, they fail to reliably quantify fugitive CO_2 emissions, further compromising the accuracy of emission inventories.

Various optical sensing techniques have been employed for CO_2 emission measurement, such as open-path tunable diode laser absorption spectrometers (TD-LAS) and non-dispersive infrared absorption (NDIR). In addition, gas chromatography is also widely used for CO_2 emission analysis. Nevertheless, TD-LAS technique only provides integrated path concentration, which increases the uncertainty of measurement results. NDIR and gas chromatography rely almost exclusively on in-flue gas sampling. And the high-temperature, high-humidity, and high-dust environment inside the flue are prone to pipeline blockage and sensor drift [5–7].

As an advanced remote sensing technology for direct CO_2 emissions measurement, range-resolved DIAL offers distinct advantages, including non-contact measurement, high spatiotemporal resolution, and real-time response. It can effectively compensate for the limitations of traditional monitoring technologies in emission accounting and in-stack sampling, providing a promising technical approach for constructing a three-dimensional monitoring system for industrial CO_2 emissions.

Previous studies have verified DIAL for CO_2 remote sensing. Howes et al. used a ground-based 2 μm band pulsed DIAL system to achieve the accurate quantitative monitoring of industrial CO_2 emission fluxes, providing a low detection limit measurement method for industrial point source carbon emission verification [8]. Parracino et al. adopted a vehicle-mounted 2 μm band pulsed DIAL device to realize the remote detection of CO_2 concentration profiles and emission fluxes in volcanic areas, offering long-distance observation support for monitoring carbon release from volcanic activities [9]. Stroud et al. employed a ground-based 1.5 μm band pulsed DIAL device to realize real-time tracking of CO_2 plumes and the inversion of emission rates in power plants, providing a plume modeling and estimation method for the dynamic monitoring of carbon emissions in the power industry [10]. Amediek et al. developed an airborne 1.57 μm band IPDA lidar to achieve the accurate acquisition of atmospheric CO_2 column concentration and strong point source fluxes, providing an airborne observation scheme for satellite-based carbon emission remote sensing verification [11]. Yue et al. integrated ground-based pulsed DIAL with coherent Doppler wind lidar to realize the synchronous inversion of local horizontal CO_2 fluxes and concentration profiles, providing a high-precision observation scheme for regional-scale carbon flux accounting [12]. Despite these progresses, most DIAL applications focus on volcanic plumes [9,13,14], urban atmospheres [13–16], or background environments [17–20], with limited field validation specifically targeting industrial stationary emission sources.

NPL has conducted important field demonstrations of DIAL for industrial gas emission measurements, with particular emphasis on facilities such as liquefied natural gas (LNG) plants [8]. These studies have provided valuable evidence for the applicability of DIAL in industrial emission monitoring. However, stationary stack CO_2 emissions in complex industrial-park environments involve different measurement challenges, including elevated stack plumes, surrounding building interference, plume-height wind correction, and the need for comparison with in-stack monitoring data. Therefore, further field validation is still needed for mobile DIAL applications targeting stationary industrial CO_2 sources.

In our previous work, we carried out controlled-release experiments and successfully measured methane emissions at 3–15 kg/h, which verified the basic capability of our DIAL system for emission-flux quantification under controlled conditions [21]. Building on these previous studies, the present work further investigates the capability of a 2 μm mobile DIAL system for quantifying CO_2 emissions from stationary industrial stacks under real field conditions. Specifically, we first captured the spatial concentration distribution of CO_2 from high-emission sources using DIAL technology. Then, we quantified the instantaneous CO_2 emission fluxes by combining wind speed and wind direction data. Finally, we performed a cross-comparison of three approaches, including DIAL detection, CEMS real-time monitoring and emission accounting, to validate the practical performance of the DIAL system in complex industrial scenarios. Compared with our previous studies, this work has carried out field tests in complex industrial park scenarios, breaking through the limitations of laboratory principle verification and controlled release experiments. Furthermore, validation experiments have been completed in three industrial scenarios with different emission intensities. This study aims to provide technical support for the practical application of DIAL technology in industrial CO_2 emission monitoring and promote the development of refined industrial carbon emission monitoring systems.

2. Theory and DIAL System

2.1. Theory

2.1.1. CO_2 Concentration

The core principle of DIAL technology for measuring CO_2 concentrations is the selective absorption of molecules at specific laser wavelengths. By emitting two laser beams—one at the absorption wavelength referred to as online (λ_{on}), where it is strongly absorbed and the other at the absorption trough, referred to as offline (λ_{off}), where little or no absorption occurs—and analyzing the difference in their attenuation during atmospheric transmission, the technology enables the quantitative inversion of CO_2 concentrations along the optical path. The transmission of laser light through the atmosphere follows the Beer–Lambert law, and the intensity of the backscattered signal can be expressed as follows [22]:

$$I(\lambda, R) = I_0(\lambda)\exp\left\{-2\int_0^R [\alpha_a(\lambda, r) + \alpha_m(\lambda, r) + N(r)\sigma(\lambda)]dr\right\}\beta(\lambda, R)R^{-2}D_x \quad (1)$$

where $I(\lambda, R)$ is the return signal intensity at distance R; $I_0(\lambda)$ is the initial laser intensity; $\alpha_a(\lambda, r)$ is the aerosol extinction coefficient; $\alpha_m(\lambda, r)$ is the atmospheric molecular scattering extinction coefficient; $N(r)$ is the CO_2 molecular number density (which is positively correlated with concentration); $\sigma(\lambda)$ is the absorption cross section of the CO_2 molecule; $\beta(\lambda, R)$ is the backscattering coefficient of the atmosphere; R^{-2} is the geometric attenuation factor; D_x is a distance-independent constant that depends solely on the DIAL system itself.

Since the selected absorption wavelength (λ_{on}) is very close to the reference wavelength (λ_{off}), the scattering characteristics of aerosols and atmospheric molecules at a distance (R) can be approximated as follows: $\alpha_a(\lambda_{on}, r) \approx \alpha_a(\lambda_{off}, r)$, $\alpha_m(\lambda_{on}, r) \approx \alpha_m(\lambda_{off}, r)$ and $\beta(\lambda_{on}, R) \approx \beta(\lambda_{off}, R)$. Therefore, these parameters can cancel each other out in the calculation of the ratio of return signal intensities at the two wavelengths $I(\lambda_{off}, R)$ and $I(\lambda_{on}, R)$, ultimately yielding the following inversion formula for the CO_2 concentration (C) [23]:

$$C = \frac{1}{2\sigma(\lambda_{on}) - 2\sigma(\lambda_{off})}\frac{d}{dR}\left[\ln\frac{I(\lambda_{off}, R)}{I(\lambda_{on}, R)}\right] \quad (2)$$

where C represents the volumetric concentration of CO_2 (in ppm); $\sigma(\lambda_{on})$ and $\sigma(\lambda_{off})$ represent the absorption cross-sections of CO_2 at wavelengths λ_{on} and λ_{off}, respectively (in cm^2/molecule); R represents the detection distance (in meters).

2.1.2. Smoke Plume Velocity

Plume transport velocity is conventionally estimated using near-surface anemometers or wind lidars. However, single-height point measurements lack vertical representativeness, and distant meteorological data introduce spatial mismatch errors. Wind lidars may be obstructed by industrial structures, limiting data reliability.

To improve flux accuracy, this study employs a logarithmic wind profile model to fit and extrapolate near-surface wind measurements to plume height [24]:

In this study, synchronous wind-speed measurements at 3 m, 6 m, and 12 m were used as inputs for the logarithmic profile fitting. This treatment follows the practical approach used in previous ground-based DIAL measurements of industrial CO_2 emissions in the 2 μm wavelength region, where wind-profile information was used to support emission-flux inversion when direct wind measurements at plume height were limited [8]. In the present study, valid observations were obtained within a short field campaign and under relatively stable meteorological conditions. Therefore, air density, temperature, pressure, and seasonal variations were not introduced as separate correction terms. Their combined influence was partly represented by the measured wind profiles, while the residual approximation error was included in the wind-field uncertainty of the flux inversion.

$$u(z) = \frac{u_z}{k} \ln\left(\frac{z-d}{z_0}\right) \tag{3}$$

where $u(z)$ is the wind speed at height z, u_z is the friction velocity, k is the Karman constant (taken as 0.4), d is the displacement height from the zero plane and z_0 is the roughness length. The wind speed at the centre of the plume is then extrapolated by fitting the observed wind speed data at three heights near the ground using the least squares method to determine $u(z)$, d, and z_0.

2.1.3. Flux Measurement

CO_2 emission flux is defined as the total mass of CO_2 passing through the plume cross-section per unit time. In this paper, we present a comprehensive inversion workflow for CO_2 emission flux from industrial sources. This workflow is based on the flux integration method and combines the two-dimensional concentration distribution of the plume, inverted using the DIAL system, with the effective plume wind speed obtained by fitting a wind profile model. A series of quality control measures are adopted during DIAL monitoring to ensure observation accuracy, and full coverage of the smoke plume is one of the key strategies. Firstly, an infrared camera was used to identify the plume profile and preliminarily set the initial scanning angle of the DIAL system. Then, the scanning angle was finely corrected and optimized based on the measured concentration distribution data. Meanwhile, the actual scanning coverage was designed to be wider than the real diffusion range of the plume to realize comprehensive detection. This approach avoids missing monitoring areas and ensures accurate and reliable results of emission flux inversion. Figure 1 illustrates this workflow.

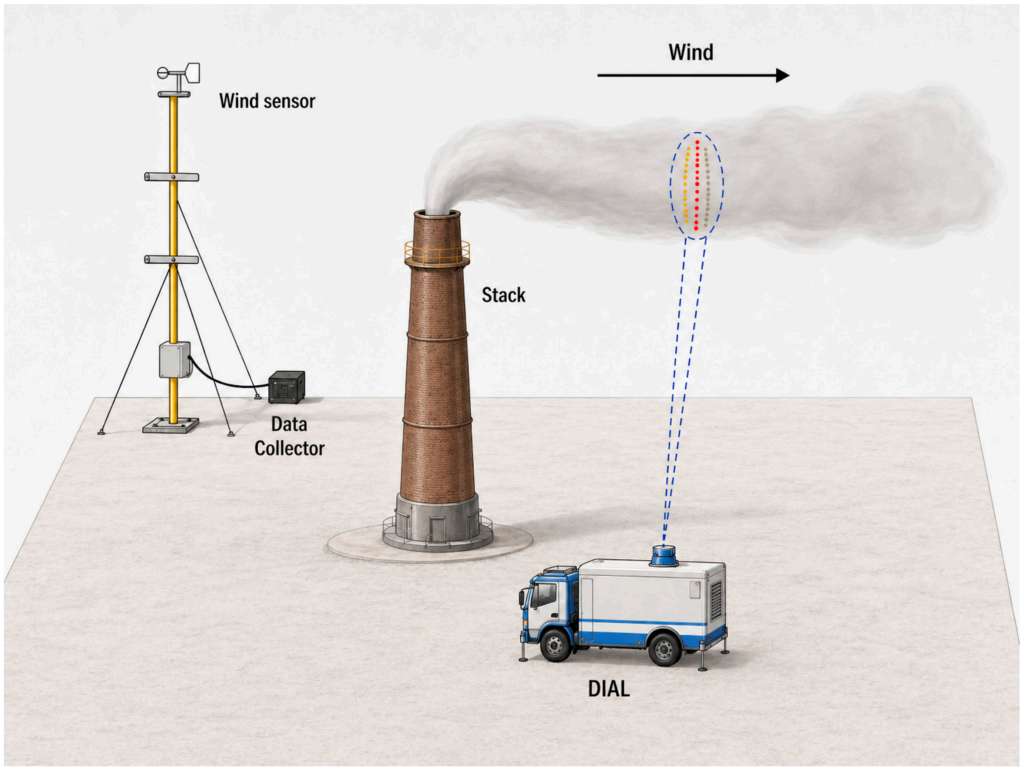


Figure 1. Schematic diagram of a DIAL measuring an industrial plume. The DIAL is positioned downwind of the emission source, with its scanning direction almost perpendicular to the plume's direction of travel. Wind speed and direction data are collected using two to four meteorological sensors.

First, multiple sets of one-dimensional 'distance–concentration' data sequences were obtained at different angles through vertical plane scanning with DIAL. These were then coordinate-mapped according to the angle of the scan and the spatial position to construct a two-dimensional data matrix of plume concentration. This data matrix was then subjected to two-dimensional smoothing and the atmospheric background CO_2 concentration downwind of the non-emission source was subtracted. This yields the cross-sectional concentration distribution of the plume attributable to industrial emissions (C(x,y)), and the effective cross-sectional area (A) of the plume is determined.

The formula for inverting the CO_2 emission flux is based on the principle of flux integration [23]:

$$F = k\iint_A C(x,y)u(x,y)\rho\cos\theta dxdy \quad (4)$$

where k: The flux conversion factor (g/s/(t/h)), taken as 3.6×10^{-3}; A: The effective cross-sectional area of the CO_2 plume (m^2), determined from the concentration distribution map; ρ: The CO_2 mass concentration conversion factor ($g/m^3 \cdot ppm^{-1}$) is taken as 1.81×10^{-3}; u(x,y): The effective wind speed at the plume height corresponding to the point (x, y) (m/s), extrapolated from the logarithmic vertical wind profile model; θ: The angle between the wind direction and the normal direction to the plume cross-section (°). This is used to correct for the effect of the wind direction on the effective wind speed, ensuring that only the wind speed component perpendicular to the cross-section is calculated.

2.2. DIAL Instruments

This paper presents a 2-μm-band, vehicle-mounted DIAL system that is fully integrated into a mobile laboratory. The system was developed by the National Institute of Metrology (China). Consisting of a laser source unit, a gas absorption cell unit and

a detection unit, the system is capable of the long-range, non-contact detection of CO_2 concentrations in industrial plumes. The core structure is shown in Figure 2.

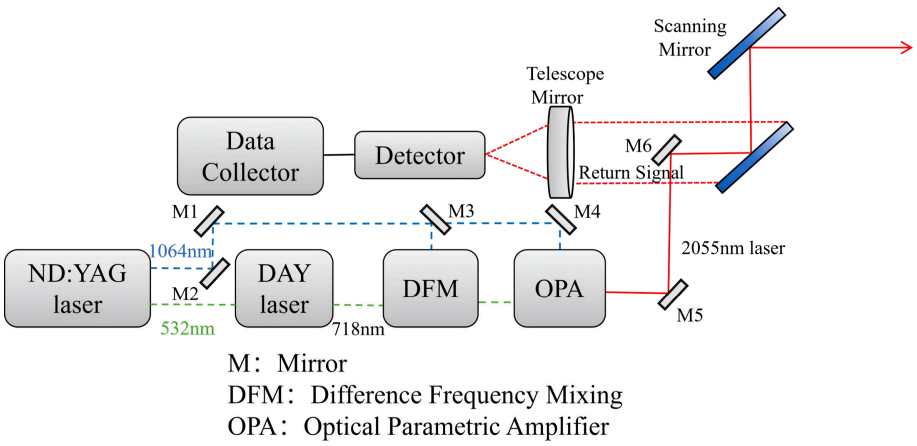


Figure 2. Schematic diagram of the DIAL system modules.

2.2.1. Laser Source Unit

CO_2 has multiple usable absorption lines around 2 μm. Based on the CO_2 absorption spectrum from the HITRAN 2020 database (296 K, 1 atm) (Figure 3), this system selects 2055 nm as the core detection wavelength to achieve optimal detection. To achieve laser output at this wavelength, the laser unit generates a pulsed CO_2 detection laser light using nonlinear optical frequency conversion technology. The system uses an Nd:YAG nanosecond pulsed laser with a seed injector as the pump source. This is capable of outputting dual-wavelength lasers at 1064 nm and 532 nm. The 532 nm pump light drives a dye laser to generate a tunable 718 nm laser. This is then combined with the 1064 nm fundamental frequency light to produce a second harmonic. This signal is finally amplified by an optical parametric amplifier (OPA) to produce a stable 2055 nm pulsed laser output.

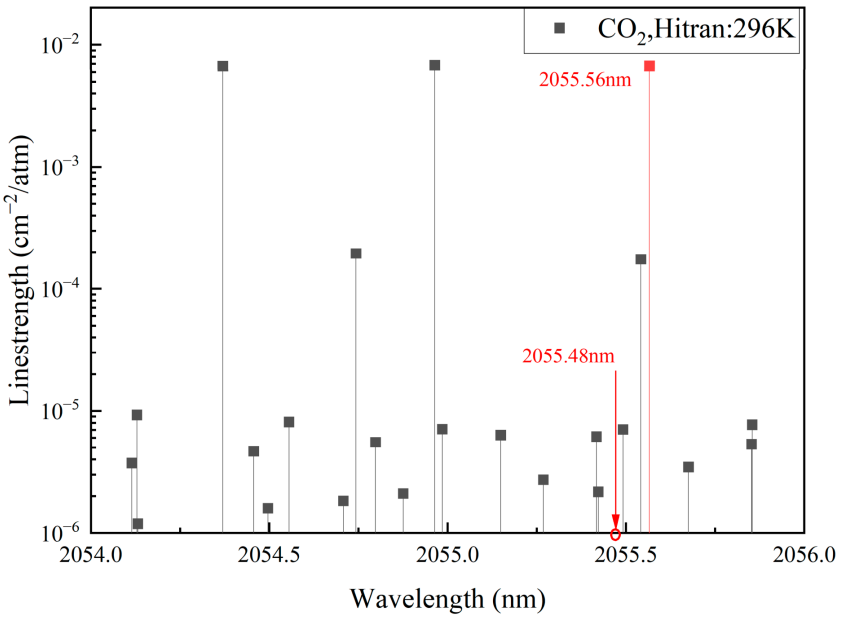


Figure 3. CO_2 absorption spectrum around 2 μm from the HITRAN 2020 database (under conditions of 296 K temperature and 1 atm standard atmospheric pressure), showing the strong absorption peak at 2055.58 nm and weak absorption trough at 2055.46 nm selected by the DIAL system.

The final laser unit stabilized its pulse energy output between 10 and 15 mJ, precisely locking the online wavelength (λ_{on}) at 2055.58 nm (corresponding to the strong absorption peak of CO_2) and setting the offline wavelength (λ_{off}) to 2055.46 nm (corresponding to the weak absorption region of CO_2).

2.2.2. Gas Absorption Unit

According to the working principle of DIAL, the differential absorption coefficient is the core parameter for achieving accurate CO_2 concentration retrieval. Currently, there are two main approaches to obtain this parameter: one is to directly calculate it using the absorption coefficient corresponding to the target wavelength from the HITRAN database [25]; the other is to in situ measure the differential absorption coefficient through a reference gas absorption cell [26]. However, direct use of the data from the HITRAN database may introduce deviations due to inconsistencies with actual field conditions. Therefore, the system integrates a reference gas cell unit: the optical path length of the gas cell is 15 cm, and it is filled with 99.99% pure CO_2 standard gas (National Institute of Metrology (Beijing)).

Figure 4a shows the measured spectrum of the output laser beam. A small fraction of the output laser was coupled into the gas absorption unit, where one part was directly detected by a pyroelectric detector, and the other part was detected by another pyroelectric detector after passing through the reference gas. According to the Beer–Lambert law, the measured absorption coefficient curve of CO_2 in the reference cell was obtained from the two detector signals. The central position and line shape of the measured absorption peak are highly consistent with the simulated spectrum based on the HITRAN database, verifying the system's ability to accurately resolve the CO_2 characteristic absorption peak and calibrate the laser wavelength.

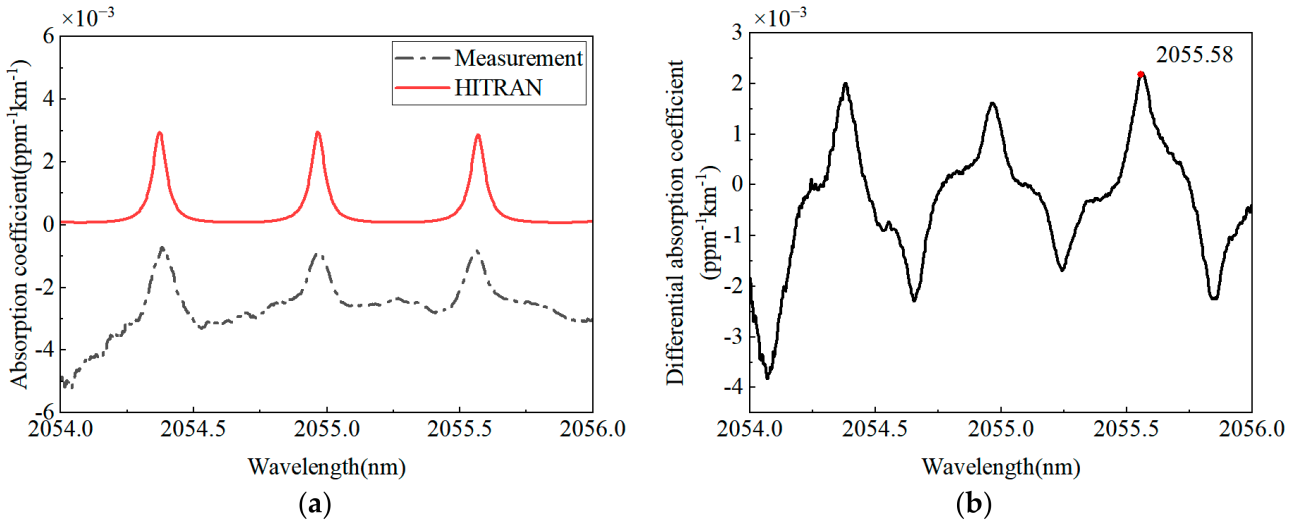


Figure 4. Laser spectroscopy test results: (**a**) A comparison of the absorption coefficient curves in the reference gas cell and in the HITRAN database. (**b**) The differential absorption coefficient curves.

Figure 4b presents the differential absorption coefficient curve derived from the transmitted light intensities of the laser at the online (λ_{on}) and offline (λ_{off}) wavelengths through the gas cell, calculated via the Beer–Lambert law. After the statistical averaging of multiple measurements, the CO_2 differential absorption coefficient applicable to this system was determined to be 2.37×10^{-3} $ppm^{-1} \cdot km^{-1}$. Calibrated from experimental measurements, this value is more consistent with the actual working state of the system than the theoret-

ical value directly adopted from the database, significantly improving the accuracy and reliability of concentration retrieval.

In addition, this system incorporates a real-time laser absorption coefficient monitoring module. Based on a reference gas cell unit, this module enables the laser emission wavelength to be monitored and calibrated in real time during actual field measurements. This prevents shifts in the wavelength caused by environmental disturbances and component drift during prolonged measurements, thereby ensuring the long-term stability of the wavelength in both online and offline modes.

2.2.3. Detection Unit

In order to effectively detect CO_2 return signals in the 2 μm band, this system uses an InGaAs PIN photodetector as its core receiving component. Its spectral response range of 0.9–2.55 μm fully encompasses the operating band of the system. The faint photocurrent signal output by the detector is amplified by a low-noise preamplifier. The amplifier gain is set to 10^4 to suppress noise and boost the weak return signal to a level suitable for acquisition. The amplified analogue signal is then transmitted to the data acquisition unit.

2.2.4. Scanning Unit

The scanning unit is used to take three-dimensional measurements of the concentration distribution across the plume cross-section. The system uses a high-precision, motorized, two-dimensional turntable as its core scanning mechanism, with an angular resolution of up to 0.05°. The scanning range covers the vertical plane from 0° to +180°. By adjusting the pitch angle, the laser beam can traverse the CO_2 emission plume precisely from different heights and angles. This ensures the laser path fully covers the plume's entire cross-section, capturing its spatial concentration distribution along the vertical profile. Ultimately, this enables the two-dimensional concentration imaging of the emission plume and precise flux inversion.

2.2.5. Key Technical Specifications of the System

The specifications of the DIAL system can be found in Table 1.

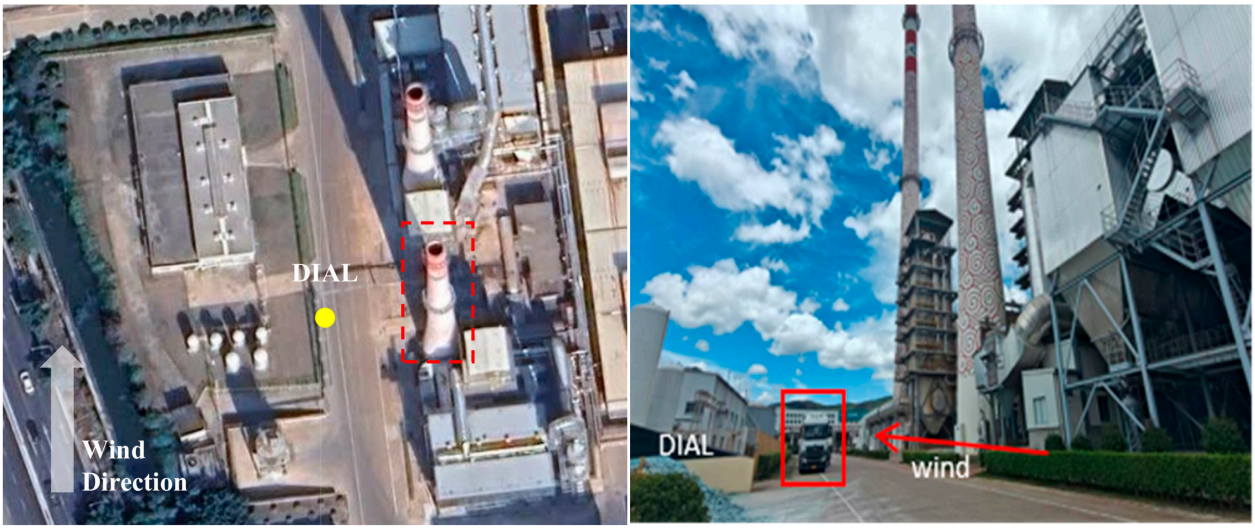
Table 1. Key Technical Specifications of DIAL.

	Parameters	Value
Laser	Pulse width	9 ns
	Repetition rate	10 Hz
	Laser energy	10 mJ
	online (λ_{on}) (CO_2 strong absorption)	2055.58 nm
	offline (λ_{off}) (CO_2 weak absorption)	2055.46 nm
Receiver	Telescope diameter	500 mm
	Divergence	~0.2 mrad
	Scanner angular precision	0.05°
Detector	Photodiode	InGaAs PIN
	Diameter	1 mm
	Photo Sensitivity	1.5×10^8 V/W
	NEP	6×10^{-13} W/$\sqrt{\text{Hz}}$
Analog-to-digital converter	Dynamic range	12 bit
	Sampling rate	40 MS·s^{-1}

3. Experiments and Results

3.1. Experimental Design

In order to verify the ability of the DIAL system to measure CO_2 emissions in industrial settings, field observation tests were conducted in September 2025 at an industrial park in Fuzhou, Fujian Province, China. As shown in Figure 5, the mobile DIAL system was positioned approximately 30 m from the stack base on the ground to obtain an unobstructed viewing path toward the plume. Under the selected scanning geometry, the detected plume core was located at a slant range of approximately 100–150 m, corresponding to an altitude of about 100–140 m. Therefore, the measurements were performed on the transported plume cross-section rather than the immediate near-stack region. This placement effectively avoided obstructions such as tall factory buildings and raw material storage yards surrounding the stack. It ensured an unobstructed laser transmission path, guaranteeing the stability and integrity of the return signals.



(a) (b)

Figure 5. Relationship between DIAL and emission sources: (**a**) Satellite diagram of the layout, where the red dashed box indicates the stack to be measured; (**b**) On-site photograph, where the red box marks the DIAL system and the red arrow indicates the wind direction.

In order to obtain a full cross-sectional view of the CO_2 plume, the scanning angle of the system was set to between 70° and 90°, which corresponds to a plume height range of between 100 and 140 m. The scanning increment was set to 1°. Each complete scan took approximately 10 min, yielding 11 concentration profiles at different elevation angles. Each profile comprised 500 laser pulse measurements (taking approximately 50 s) to ensure a sufficient signal-to-noise ratio. Three wind speed and direction sensors were deployed concurrently during the experiment and installed at heights of 3 m, 6 m, and 12 m, respectively. Each sensor recorded a set of wind speed and direction data every minute, providing high-precision meteorological support for the subsequent determination of effective wind speeds within the plume.

In addition, a CEMS has been installed in the stack flue. This system uses non-dispersive infrared absorption spectroscopy to monitor CO_2 concentrations in real time, providing a reliable reference for the DIAL measurement results. Meanwhile, in collaboration with staff from companies within the industrial park, we obtained manual records of fuel consumption and other data from the same period. These records were used for carbon emissions accounting and to cross-validate the results.

To improve measurement accuracy and ensure the integrity of lidar observations, all tests were performed in strict accordance with the following quality control procedures:

1. Wavelength accuracy and drift control are critical for DIAL detection. A reference gas cell was adopted for real-time online monitoring during measurement to effectively avoid spectral wavelength offset.
2. Wind speed and wind direction were monitored synchronously in real time. Observation data were eliminated when the wind speed was lower than 1 m/s, the included angle between wind direction and scanning direction was less than 30°, or unstable wind field fluctuations were identified through the manual visual screening of meteorological time-series records. Significant abnormal data caused by rainfall and extreme weather were directly excluded.
3. If the first or last scanning line of the acquired concentration distribution profile intersected with the plume boundary, the corresponding data would also be eliminated.

To verify versatility, additional tests were carried out at a photovoltaic glass plant and a coal-fired power plant (Section 3.4).

3.2. DIAL Experimental Results

3.2.1. DIAL Concentration Measurement

Figure 6a shows the normalized return signals received by the DIAL system, where the signal intensity is normalized to the real-time monitored laser output power from the gas cell unit. However, due to atmospheric turbulence, detector noise and environmental clutter, the single-pulse laser echo exhibits a high noise level and low signal-to-noise ratio. This makes it unsuitable for direct concentration inversion. Therefore, this study employs a pulse cumulative averaging method to denoise the raw return signals. Arithmetic averaging is performed on 250 online wavelength (λ_{on}) and 250 offline wavelength (λ_{off}) pulse return signals to significantly suppress random noise and improve the signal-to-noise ratio of the useful signal. The spikes that appear in the initial segment of the signal are caused by internal stray light within the system. They do not fall within the effective detection range and therefore have no impact on smoke plume concentration inversion. Substituting the denoised online and offline return signals into DIAL inversion Equations (1) and (2) enables the calculation of distance-resolved CO_2 concentration profiles, as illustrated in Figure 6b. As can be seen in the figure, the atmospheric background CO_2 concentration is ~400 ppm, within the range of 100–150 m, the laser beam passes through the emission plume and the concentration signal shows a significant increase, which is consistent with the actual spatial location of the plume.

The path-integrated concentrations of all scan profiles were differentiated based on the concentration inversion of a single path to obtain a complete distance-resolved concentration distribution, as shown in Figure 7a. For a single angular position, each concentration profile was obtained by accumulating 500 laser pulses (250 online + 250 offline pulses), with a system repetition rate of 10 Hz, resulting in a total measurement time of ~50 s for a single profile. Furthermore, the distance-resolved concentrations from multiple elevation-angle scan profiles were spatially georeferenced and data-merged. Two-dimensional smoothing and interpolation algorithms were then applied to optimize the spatial distribution patterns, ultimately reconstructing the two-dimensional concentration field distribution of the smoke plume cross-section (Figure 7b). These reconstruction results intuitively reflect the dispersion pattern of the plume, the location of concentration peaks and the lateral distribution range. This provides reliable two-dimensional concentration data for the subsequent precise calculation of emission fluxes.

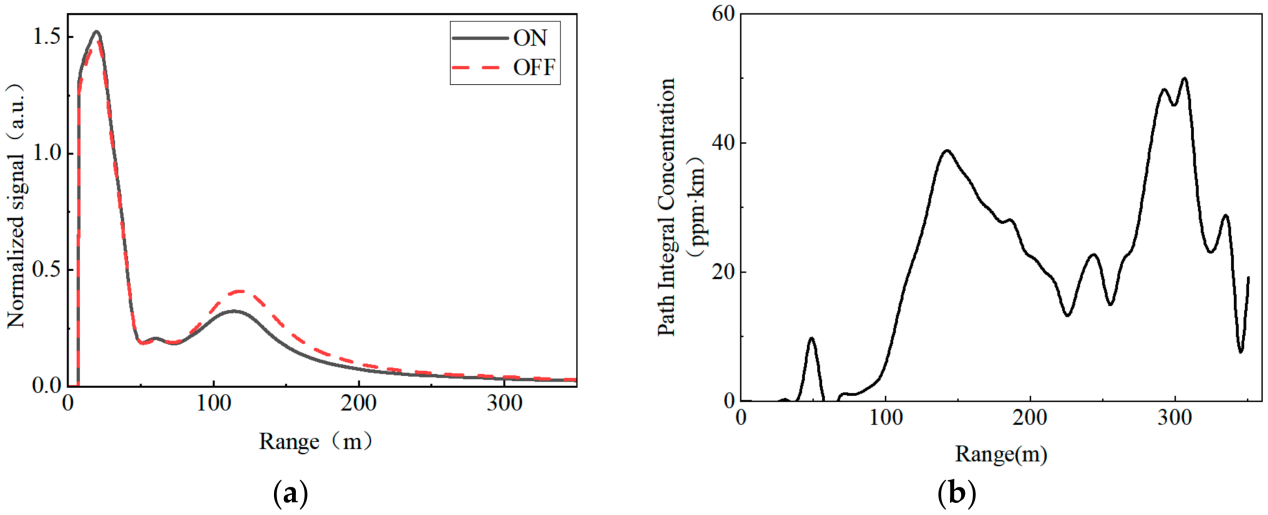


Figure 6. DIAL return signals and path-integrated CO_2 concentration. (**a**) Normalized online and offline return signals, with the vertical axis representing normalized signal intensity in arbitrary units (a.u.). (**b**) Path-integrated CO_2 concentration along the laser path, the plume-induced concentration enhancement located at 100–150 m distance.

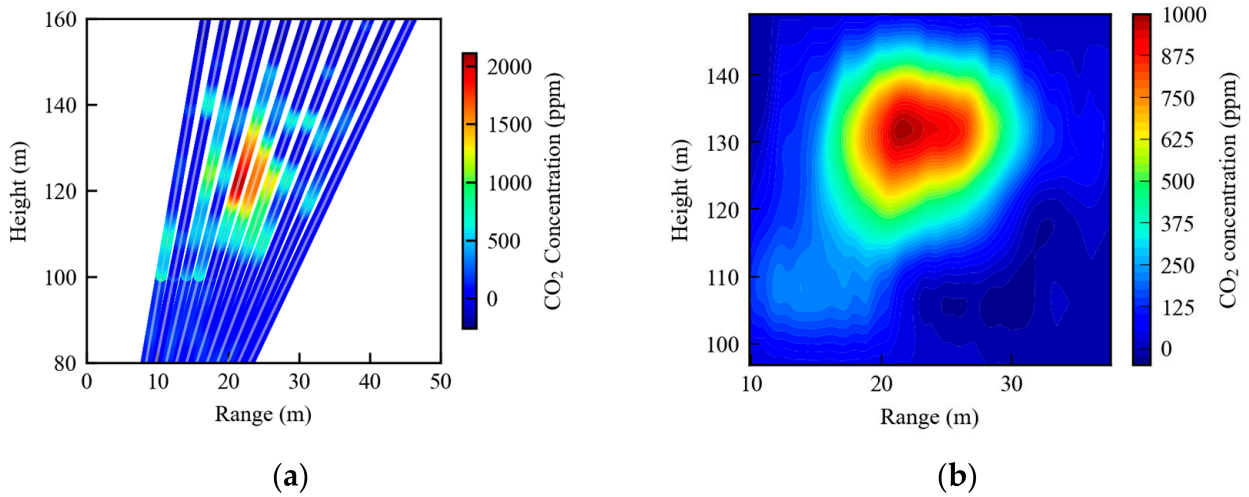


Figure 7. Two-dimensional DIAL concentration distribution. (**a**) Distance-resolved concentrations from multiple scan profiles; (**b**) Two-dimensional concentration distribution obtained by realigning and smoothing the scan profiles.

Figure 7b illustrates the two-dimensional distribution of smoke plume concentrations, as derived from DIAL inversion. As can be seen in the figure, the smoke plume's high-concentration core is located within the altitude range of 110–130 m and the horizontal range of 0–20 m. This corresponds to the main plume area downwind of the stack outlet. The concentration peak reaches 930 ppm, clearly demonstrating the characteristic concentration of CO_2 emissions from natural gas combustion. Outward from the core zone to the diffusion region (altitudes of 100–110 m and 130–140 m and horizontal distances of 20–50 m), the CO_2 concentration gradually decreases to 410 ppm. This distribution pattern is highly consistent with the dilution characteristics of a plume under turbulent atmospheric diffusion. At the same time, the DIAL system clearly identifies local zones of high concentration within a horizontal range of 10–15 m and a vertical range of 120–125 m, which demonstrates the system's capability to resolve fine-scale plume structures. The system is capable of comprehensively characterizing the concentration details across the plume cross-section

and provides reliable, complete cross-sectional concentration data to support the accurate integration of emission flux calculations in subsequent analyses.

3.2.2. Quantification of DIAL Emissions

Figure 8 shows the vertical wind profile fitted from the near-surface wind-speed measurements at 3 m, 6 m, and 12 m, with a coefficient of determination R^2 of 0.9852 and a 95% confidence interval of the fitted parameters ranging from [0.51, 1.13] for the slope and [−0.51, 0.46] for the intercept. Field measurements are not advisable at wind speeds below 1 m/s, as weak wind conditions result in slow plume diffusion. To improve the accuracy of carbon emission flux calculations further and ensure that the inversion results accurately reflect the actual transport state of the smoke plume, this study strictly adhered to Equation (4) for data verification. As the smoke plume exhibits distinct vertical stratification during transport, with significant differences in wind speed and direction at different altitudes, using wind speeds from a single altitude would introduce substantial errors. Therefore, it is essential to use wind speed and direction data corresponding to the actual altitude of the smoke plume. Based on this, the study used a wind profile model to fit and extrapolate the measured wind speeds in order to obtain the effective wind speed and direction distributions within the smoke plume's height range. This ensures that each set of emission calculation results can be matched with a corresponding real-time wind profile, thereby significantly improving the reliability and stability of flux calculations. This provides more representative wind-speed and wind-direction inputs for flux inversion than single-height wind measurements.

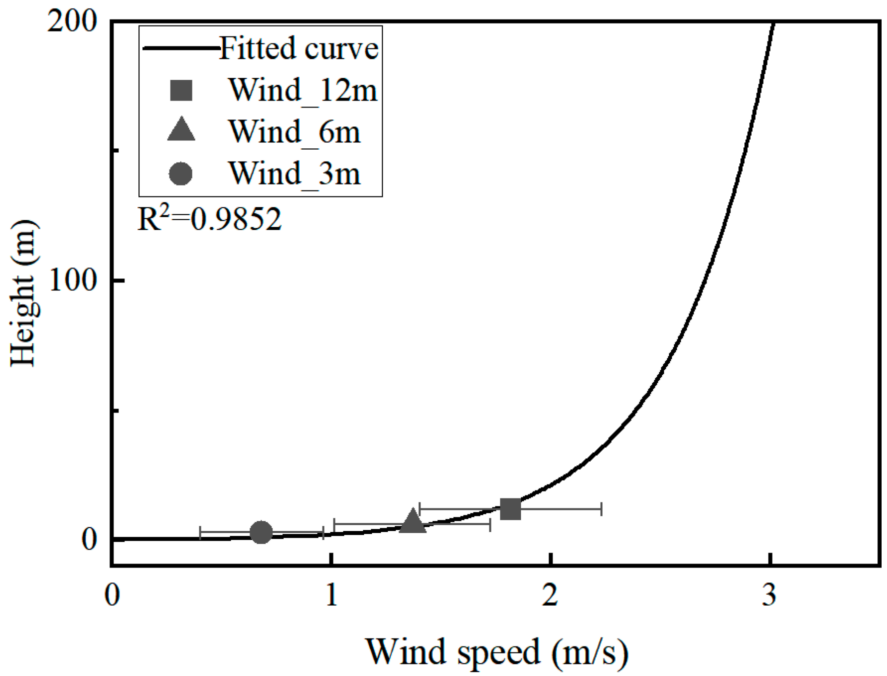


Figure 8. Vertical wind profile fitted by the logarithmic wind model within the first 300 m above ground level. The black symbols (circles, triangles, and squares) represent wind speed measurements at 3 m, 6 m, and 12 m heights collected by near-surface anemometers; the black solid line is the fitted logarithmic wind profile curve; the horizontal error bars indicate the standard deviation of wind speed data at the corresponding height during a single DIAL emission measurement cycle (approximately 10 min).

A total of 27 valid scans were completed during the experiment. Due to adverse weather conditions, including low wind speeds and rainfall, on the second day, the data from that period exhibited significant anomalies and were excluded following quality

control. Table 2 details the experimental conditions, meteorological and environmental parameters for each valid observation day. Atmospheric stability was approximately estimated according to wind speed and daytime meteorological conditions during the measurement period.

Table 2. Experimental conditions and meteorological parameters for each measurement day.

Test	Valid Scans	Average Wind Speed (m/s)	Average Wind Direction (°)	Temperature (°C)	Relative Humidity (%)	Atmospheric Pressure (hPa)	Atmospheric Stability
1	7	2.89	189.91	34	85	1006	Neutral
2	6	2.06	173.71	33	90	1005	Neutral
3	7	2.37	186.62	35	80	1004	Slightly Unstable
4	7	2.53	192.86	34	90	1003	Neutral

Figure 9 presents the CO_2 emission flux measurement results corresponding to the 27 sets of valid scans. For each scan, the emission flux was calculated by integrating the reconstructed two-dimensional CO_2 concentration distribution with the plume-height wind speed according to Equation (4). The measured fluxes ranged from 9523.04 to 11,876.91 kg/h, with an overall mean of 10,528.14 kg/h and a standard deviation of 762.03 kg/h. To provide a basic statistical comparison among the four measurement days, the Shapiro–Wilk test was first used to examine the normality of the daily flux datasets. The results showed no significant departure from normality for each group ($p > 0.05$). A one-way ANOVA was then applied to compare the daily mean fluxes, and no statistically significant difference was observed among the four groups ($F = 2.274$, $p = 0.066$). The coefficient of variation for all valid scans was 7.24%, indicating the acceptable short-term repeatability and consistency of the DIAL-derived emission estimates under the selected field conditions.

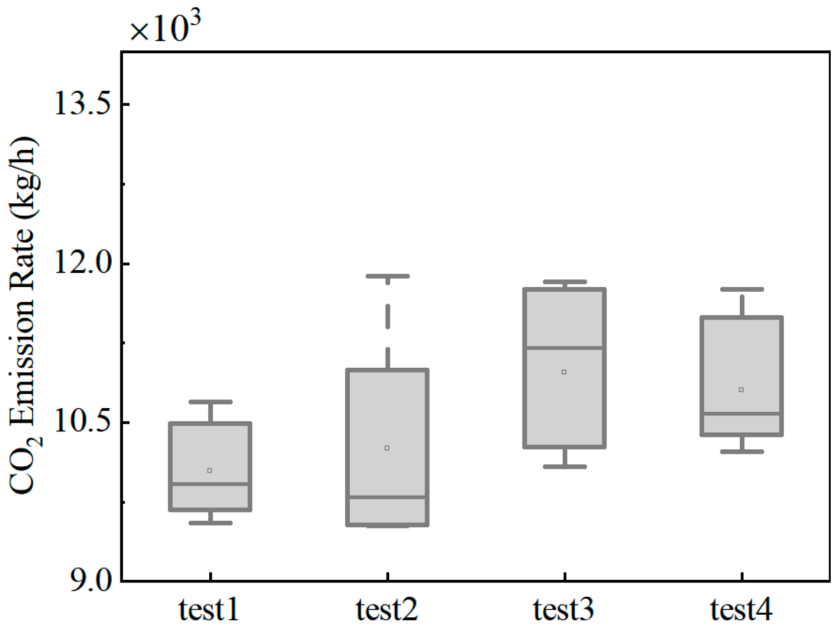


Figure 9. DIAL measures industrial plume emissions.

3.2.3. Evaluation of Uncertainty Sources

The uncertainty of CO_2 emission flux mainly originates from five independent components: the systematic uncertainty of CO_2 concentration, the statistical uncertainty of concentration retrieval, wind speed uncertainty, wind direction uncertainty, and the measurement repeatability uncertainty of emission flux [27,28].

The systematic uncertainty of CO_2 concentration is primarily caused by the deviation of differential absorption coefficient calibration and laser wavelength calibration. Combined with the calibration results of high-purity CO_2 gas cells, the relative systematic uncertainty is determined to be 0.89%.

The statistical uncertainty of concentration retrieval arises from the range-dependent decrease in the signal-to-noise ratio of the return signal, and is approximately 3.00% within the effective detection range of 50–200 m.

Through the root-sum-square synthesis of systematic and statistical components, the total relative uncertainty of concentration is calculated to be 3.13%.

Wind field uncertainty is introduced by meteorological observation and logarithmic wind profile fitting. The relative uncertainty of wind speed is 14.07%, and the relative uncertainty of wind direction is 3.93%. The combined relative uncertainty of the wind field is 14.61%.

The relative uncertainty of emission flux measurement repeatability obtained from multiple repeated scanning tests is 7.23%.

Assuming that each uncertainty component is independent of each other, the total uncertainty of CO_2 flux retrieved by DIAL is synthesized through the root-sum-square method:

$$u_r(F) = \sqrt{u_r(C)^2 + u_r(Wind)^2 + u_r(Repeat)^2} \quad (5)$$

Substituting each component for calculation, the combined relative standard uncertainty of flux is 16.60%. When the coverage factor k = 2, the relative expanded uncertainty is 33.20%.

3.3. Comparison of Results

Table 3 compares daily average CO_2 emission rates from DIAL, CEMS, and the emission-factor method. Values after ± indicate standard deviations for repeated DIAL and CEMS measurements. CEMS performs in situ continuous measurement inside the flue duct with minimal interference from the external environment, thus yielding measurement results with low dispersion and a narrow error range. In contrast, DIAL conducts non-contact measurements in the open atmospheric environment, which are susceptible to stochastic factors including fluctuations in on-site meteorological conditions and variations in plume diffusion morphology, resulting in a relatively wider error range. For this reason, the emission level is evaluated using the mean value of multiple repeated scans to avoid the misjudgment of results caused by the upper and lower limits of single measurements.

Table 3. Comparison of DIAL, CEMS and Calculation Method Results, (±) represent the standard deviation of repeated measurements.

Test	DIAL	CEMS	Calculation	Units
1	10,038.62 ± 427.39	10,472.22 ± 113.99	11,315.95	kg/h
2	10,251.81 ± 966.84	10,886.53 ± 118.08	11,073.54	kg/h
3	10,974.16 ± 724.45	10,699.26 ± 196.00	10,798.64	kg/h
4	10,808.47 ± 591.76	10,925.57 ± 169.52	10,841.52	kg/h

The results show that the measurement results of the three methods have good consistency, among which DIAL and CEMS measurements are matched with no significant systematic deviation. During the four-day observation period, the average CO_2 emission rate measured by the DIAL system was 10,528.14 kg/h, while that measured by the CEMS system was 10,740.69 kg/h. Meanwhile, the average CO_2 emission rate calculated by the emission factor method (compliant with the IPCC Guidelines and Chinese national

standard specifications) was 11,013.49 kg/h, with an overall average relative deviation of +2.54% from the CEMS benchmark value and +4.61% from the DIAL measurements, which further corroborates the reliability of the field measurement results.

To further quantitatively evaluate the measurement accuracy of the DIAL system, we calculated the relative deviation of the daily average emission rate for each test and the total root mean square error (RMSE) with CEMS as the benchmark. The results are as follows: the relative deviation was −4.14% for Test 1, −5.83% for Test 2, +2.57% for Test 3, and −1.07% for Test 4, with the relative deviation of all test days controlled within ±6%. The total RMSE of the full test period (Test 1 to Test 4) was 412.36 kg/h, accounting for only 3.92% of the average emission rate. Based on 27 valid scans during the test period, the coefficient of variation (CV) of the DIAL measurements was 7.24%, indicating that the DIAL system can provide repeated emission estimates that are broadly consistent with CEMS under the selected valid meteorological conditions. The above results support the effectiveness and applicability of the DIAL technology developed in this study for CO_2 emission monitoring from stationary industrial sources.

3.4. Field Application to Additional Industrial Sources

To further explore the applicability of the developed DIAL system across industrial scenarios with different emission intensities, we conducted field tests at two representative sites: a glass manufacturing plant (representative of low emission intensity and steady-state operating conditions) and a coal-fired power plant (representative of high emission intensity and dynamic load conditions). The core objectives of the tests were as follows: to verify the system's capability to measure CO_2 emission rates across different orders of magnitude, to evaluate its performance in capturing the dynamic characteristics of emission variations, and to provide data support for the standardized application of DIAL technology in industrial carbon accounting.

3.4.1. Photovoltaic Glass Manufacturing Plant

Field tests were carried out at a glass production base from 6–7 September 2025. The base is equipped with a natural gas-fired glass melting furnace, whose carbon emissions are mainly derived from the natural gas combustion process, making it an ideal subject for verifying the measurement performance of the DIAL system for fuel combustion emission sources.

During the test period, the plant was in its annual scheduled maintenance shutdown. The melting furnace was operated at low load for heat preservation, with no large-scale raw material feeding or glass forming operations, resulting in relatively stable emission conditions. The DIAL system was deployed in the area southeast of the plant boundary, with a horizontal distance of 100 m from the main stack, which has an outlet height of 95 m. The scanning path covered the core cross-section of the plume dispersion. The test was operated continuously for 5 h, and a total of five sets of valid CO_2 emission rate data were acquired. Figure 10 shows the temporal variation trend of CO_2 emission rates during the test period. Statistical results show that the emission rates ranged from 1824 to 2135 kg/h, with a mean value of 2028.60 ± 127.31 kg/h (±1σ).

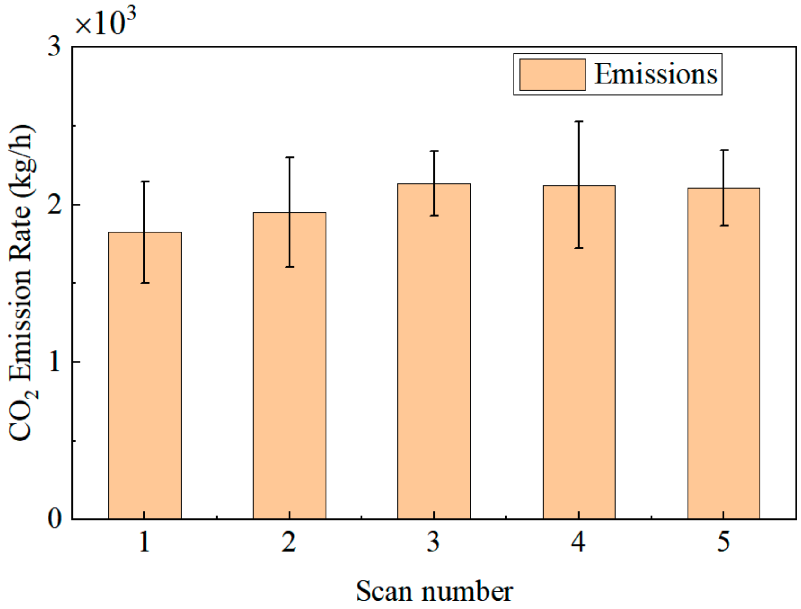


Figure 10. Temporal variation of CO_2 emission rates measured by the DIAL system at the glass manufacturing plant (6–7 September 2025).

3.4.2. Coal-Fired Power Plant

To evaluate the performance of the DIAL system in scenarios with high emissions and strongly dynamic load fluctuations, we conducted field tests at a coal-fired power plant on 17 September 2025. Flue gas from the plant's two 500 MW subcritical condensing generator sets, which use bituminous coal as the design fuel, was discharged through a 240 m high stack after treatment via flue gas desulfurization (FGD), denitrification, and dust removal systems. The DIAL system was deployed 50 m east of the stack base, and a sector scanning mode was adopted for the system. The vertical scanning range fully covered the stack outlet; to ensure the complete coverage of the plume dispersion cross-section, we set a significantly wider scanning range than in previous tests, covering an angle of approximately 25° to 30°. The test lasted for 6 h, and a total of six sets of valid data were acquired.

Figure 11 shows the temporal variation trend of CO_2 emission rates at the coal-fired power plant. Statistical results show that the hourly-averaged emission rates ranged from 530,806 to 611,061 kg/h, with an overall mean of 570,524 ± 32,245 kg/h (±1σ).

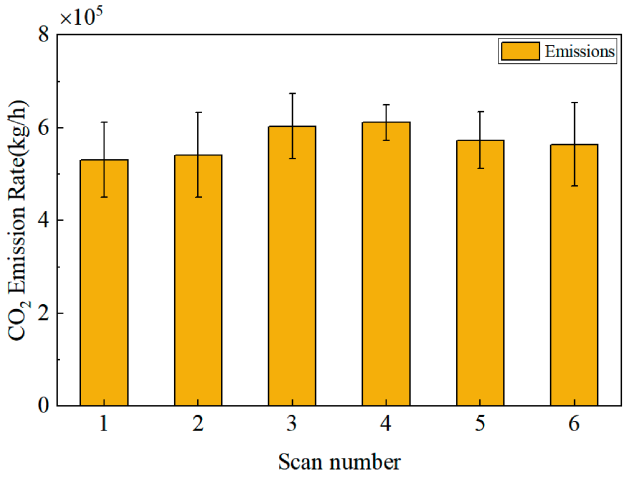


Figure 11. Temporal variation of CO_2 emission rates measured by the DIAL system at the coal-fired power plant (17 September 2025).

4. Discussion

This study demonstrates the feasibility of DIAL for the remote measurement of industrial CO_2 emissions and highlights its potential application in industrial emission monitoring. Compared with our team's previous methane DIAL monitoring research and similar international work, this study extends DIAL to the field of industrial CO_2 emission monitoring and completes field verification in three types of industrial scenarios with different emission intensities.

In Section 3.2.3, we conducted a preliminary uncertainty analysis of the flux inversion sources. It should be noted that there is currently no unified standardized evaluation protocol for DIAL systems. Quantitative results demonstrate that the uncertainty arising from wind field measurement and extrapolation is the dominant error source for flux inversion. This high contribution ratio is fundamentally attributed to two interrelated factors: the inherent uncontrollability of wind speed in open atmospheric environments and the limitations of the logarithmic wind profile extrapolation method when applied in complex industrial scenarios. Although we adopted roughness parameters consistent with the empirical range for large-scale industrial parks, the discrete high-rise stacks, factory buildings and equipment at the test site form a typical non-uniform underlying surface. This induces local turbulence and causes the vertical wind profile to deviate from the ideal logarithmic law. Furthermore, the current wind speed observations are limited to only three measurement points within 3–12 m above the ground, and long-distance extrapolation to the plume center heights of 100–300 m inevitably amplifies the fitting error. More importantly, direct verification of the extrapolation accuracy using full-height wind profile measurement data was not performed in this experiment, which further increases the uncertainty of wind field correction.

The good agreement between DIAL and CEMS measurements confirms that mobile DIAL can serve as a reliable complementary method to traditional industrial carbon accounting systems. The emission factor method enables rapid macro-scale emission estimation but suffers from $\pm$10% to $\pm$30% inherent uncertainties and cannot quantify fugitive emissions. In-stack CEMS provides continuous monitoring of organized emissions but is limited to fixed stacks and cannot detect leaks from equipment, yards or storage tanks. In contrast, DIAL features non-contact remote sensing, rapid mobile deployment, and two-dimensional plume imaging. Under suitable scanning and meteorological conditions, it has the potential to support the remote quantification of organized plume emissions and certain fugitive emission sources, thereby complementing existing industrial carbon monitoring approaches. Nevertheless, the routine long-term continuous operation of DIAL may be constrained by system cost, operational complexity, and meteorological sensitivity. Its optimal application mode is to form a multi-level system with CEMS and emission factor methods: CEMS for daily fixed-point monitoring, DIAL for CEMS verification and fugitive emission quantification, and emission factor methods for macro inventory compilation, which jointly improves the accuracy and completeness of industrial carbon accounting.

This study still has certain limitations. First, the controlled release experiment of CO_2 standard gas has not been carried out, and the metrological calibration cannot be completed under controllable conditions. Relevant tests will be supplemented by referring to the team's methane-controlled release scheme in the future. Second, the near-field echo of the system has optical stray light interference. Although it does not affect the effective detection results of the plume, it still needs to be further suppressed by optimizing the optical shading and shielding design. Third, the observation period of this study is relatively short, long-term continuous verification under different meteorological conditions has not been carried out, and relevant tests will be supplemented in the follow-up.

5. Conclusions

This study successfully achieved quantitative monitoring of CO_2 emission fluxes from industrial sources using a 2-μm band DIAL system. Obtaining the two-dimensional concentration distribution of the plume and combining it with wind profile fitting enabled a quantitative inversion of CO_2 emissions from industrial plumes. Through further comparison with traditional emission accounting methods, a multi-source cross-verification system was constructed. The coefficient of variation for 27 valid scans was 7.24%, indicating good measurement repeatability and the stability of the system under complex industrial conditions.

The comparison results show that the DIAL-derived emission estimates were broadly consistent with CEMS under the selected valid measurement conditions, with a relative deviation of daily average emission rates controlled within ±6%, and a total root-mean-square error of 3.92%. These results support the measurement accuracy and field feasibility of the system under the tested conditions. Further error analysis indicates that wind speed and direction fluctuations are the primary contributors to measurement variability, while concentration fluctuations are a secondary factor.

Moreover, the mobile DIAL system was successfully applied to two additional typical industrial scenarios (a glass manufacturing plant and a coal-fired power plant), demonstrating its preliminary applicability across emission scenarios with different intensities, although further long-term and multi-site validation remains necessary. This technology offers a promising supplementary method for the verification of industrial greenhouse gas emissions.

This short-term test validates the feasibility of the mobile DIAL system for industrial CO_2 monitoring; long-term continuous operation stability and extended multi-scenario applications will be further verified in future work.

Author Contributions: Conceptualization, J.Z. and H.L.; methodology, J.Z. and L.W.; software, L.W.; validation, L.W., W.S. and J.Z.; formal analysis, W.S.; investigation, L.W.; resources, J.Z.; data curation, L.W.; writing—original draft preparation, L.W. and J.Z.; writing—review and editing, J.Z.; visualization, W.S.; supervision, M.W.; project administration, H.W.; funding acquisition, H.L. All authors have read and agreed to the published version of the manuscript.

Funding: This research was funded by National Key Technologies Research and Development Program of China, Grant No. 2023YFE0207200, and The Key Basic Operating Fund Project of the National Institute of Metrology, China, Grant No. AKYZD2512-1 and Grant No. AKYZD2207-3. The APC was funded by The National Key Technologies Research and Development Program of China, Grant No. 2023YFE0207200; The Key Basic Operating Fund Project of the National Institute of Metrology, China, Grant No. AKYZD2512-1.

Data Availability Statement: The data that support the findings of this study are available from the corresponding author upon reasonable request.

Acknowledgments: We extend our sincere gratitude to the National Metrology Institute for its invaluable support in providing instruments, platforms, experimental materials, and other resources for this work.

Conflicts of Interest: The authors declare no conflicts of interest.

References

1. Intergovernmental Panel on Climate Change (IPCC). *Climate Change 2021—The Physical Science Basis: Working Group I Contribution to the Sixth Assessment Report of the Intergovernmental Panel on Climate Change*; Cambridge University Press: Cambridge, UK, 2023.
2. Yang, Y.; Zhou, M.; Wang, W.; Ning, Z.; Zhang, F.; Wang, P. Quantification of CO_2 Emissions from Three Power Plants in China Using OCO-3 Satellite Measurements. *Adv. Atmos. Sci.* **2024**, *41*, 2276–2288. [CrossRef]
3. Liu, X.; Liu, J.; Dou, C. Uncertainty Analysis of Provincial Carbon Emission Inventories: A Comparative Assessment of Emission Factors Sources. *Sustainability* **2025**, *17*, 4787. [CrossRef]

4. Kim, C.; Lee, J.; Koh, M.; Son, S.-N. Analysis of Error Factors in Regional Ghg Estimation Based on Fuel Consumption: Focus on the Road Transport Sector. In *Proceedings of the 24th International Multidisciplinary Scientific GeoConference SGEM 2024*; SWS Publisher: Vienna, Austria, 2024; pp. 249–256.
5. Dong, W.; Sasaki, K.; Zhang, H.; Wang, Y.; Zhang, X.; Sugai, Y. Environmental Effects on NDIR-Based CH4 Monitoring: Characterization and Correction. *Environ. Sci. Technol.* **2025**, *59*, 4951–4961. [CrossRef] [PubMed]
6. Xin, W.; Yong, Y.; Qizhen, L. Comparative Analysis of Continuous Automated Ambient Air Carbon Dioxide Monitoring Systems Based on Different Principles. *Environ. Monit. Forewarning* **2025**, *17*, 74–82. [CrossRef]
7. Tauber, J.; Parravicini, V.; Svardal, K.; Krampe, J. Quantifying Methane Emissions from Anaerobic Digesters. *Water Sci. Technol.* **2019**, *80*, 1654–1661. [CrossRef] [PubMed]
8. Howes, N.; Innocenti, F.; Finlayson, A.; Dimopoulos, C.; Robinson, R.; Gardiner, T. Remote Measurements of Industrial CO_2 Emissions Using a Ground-Based Differential Absorption Lidar in the 2 Mm Wavelength Region. *Remote Sens.* **2023**, *15*, 5403. [CrossRef]
9. Parracino, S.; Santoro, S.; Fiorani, L.; Nuvoli, M.; Maio, G.; Aiuppa, A. The BrIdge voLcanic LIdar—BILLI: A Review of Data Collection and Processing Techniques in the Italian Most Hazardous Volcanic Areas. *Appl. Sci.* **2020**, *10*, 6402. [CrossRef]
10. Stroud, J.R.; Dienstfrey, W.J.; Plusquellic, D.F. Study on Local Power Plant Emissions Using Multi-Frequency Differential Absorption LIDAR and Real-Time Plume Tracking. *Remote Sens.* **2023**, *15*, 4283. [CrossRef]
11. Amediek, A.; Ehret, G.; Fix, A.; Wirth, M.; Büdenbender, C.; Quatrevalet, M.; Kiemle, C.; Gerbig, C. CHARM-F—A New Airborne Integrated-Path Differential-Absorption Lidar for Carbon Dioxide and Methane Observations: Measurement Performance and Quantification of Strong Point Source Emissions. *Appl. Opt.* **2017**, *56*, 5182. [CrossRef]
12. Yue, B.; Yu, S.; Li, M.; Wei, T.; Yuan, J.; Zhang, Z.; Dong, J.; Jiang, Y.; Yang, Y.; Gao, Z.; et al. Local-Scale Horizontal CO_2 Flux Estimation Incorporating Differential Absorption Lidar and Coherent Doppler Wind Lidar. *Remote Sens.* **2022**, *14*, 5150. [CrossRef]
13. Rossi, R.; Di Giovanni, D.; Malizia, A.; Gaudio, P. Measurements of Vehicle Pollutants in a High-Traffic Urban Area by a Multiwavelength Dial Approach: Correlation between Two Different Motor Vehicle Pollutants. *Atmosphere* **2020**, *11*, 383. [CrossRef]
14. Lan, L.; Ghasemifard, H.; Yuan, Y.; Hachinger, S.; Zhao, X.; Bhattacharjee, S.; Bi, X.; Bai, Y.; Menzel, A.; Chen, J. Assessment of Urban CO_2 Measurement and Source Attribution in Munich Based on TDLAS-WMS and Trajectory Analysis. *Atmosphere* **2020**, *11*, 58. [CrossRef]
15. Han, G.; Xu, H.; Gong, W.; Liu, J.; Du, J.; Ma, X.; Liang, A. Feasibility Study on Measuring Atmospheric CO_2 in Urban Areas Using Spaceborne CO_2-IPDA LIDAR. *Remote Sens.* **2018**, *10*, 985. [CrossRef]
16. Queißer, M.; Burton, M.; Granieri, D. Large-Area Quantification of Subaerial CO_2 Anomalies with Portable Laser Remote Sensing and 2D Tomography. *Lead. Edge* **2018**, *37*, 222a1–222a9. [CrossRef]
17. Hu, Y.; He, X.; Zhou, K.; Hong, Y.; Zhai, X.; Zhang, H.; Chen, X.; Wang, X.; Wen, Q. High-Resolution Vertical Profiling and Source Apportionment of CO_2 Using Coherent Differential Absorption Lidar in Coastal Urban Atmosphere. *Atmos. Res.* **2026**, *330*, 108556. [CrossRef]
18. Hua, Z.; Huang, J.; Shi, D.; Yuan, K.; Hu, S.; Wang, Y. Slant Detection and Error Analysis of Atmospheric Carbon Dioxide Profile with a Continuous-Wave Differential Absorption Lidar. *Opt. Lasers Eng.* **2025**, *186*, 108808. [CrossRef]
19. Zhu, T.; Xue, B.; Li, H.; Wang, Z.; Chen, C. Spatiotemporal Detection of the Carbon Dioxide Using a Compact Differential Absorption LiDAR. *Microw. Opt. Technol. Lett.* **2025**, *67*, e70184. [CrossRef]
20. Cheng, Y.; Yu, J.; Kong, Z.; Mei, L. Diode-Laser Based Field Deployable Continuous-Wave Differential Absorption Lidar for Atmospheric NO_2 Monitoring. *Opt. Lasers Eng.* **2024**, *181*, 108344. [CrossRef]
21. Zang, J.; Wu, L.; Lin, H. Investigation on Methane Emission Measurement by Differential Absorption Lidar. *Acta Metrol. Sin.* **2025**, *46*, 1520–1526. [CrossRef]
22. Lidar: Range-Resolved Optical Remote Sensing of the Atmosphere | Springer Nature Link. Available online: https://link.springer.com/book/10.1007/b106786 (accessed on 10 March 2026).
23. Robinson, R.; Gardiner, T.; Innocenti, F.; Woods, P.; Coleman, M. Infrared Differential Absorption Lidar (DIAL) Measurements of Hydrocarbon Emissions. *J. Environ. Monit.* **2011**, *13*, 2213. [CrossRef]
24. Barnéoud, P.; Ek, N. On the Application of Linear Regression to Surface-Layer Wind Profiles for Deducing Roughness Length and Friction Velocity. *Bound. Layer Meteorol.* **2020**, *174*, 327–339. [CrossRef]
25. Gordon, I.E.; Rothman, L.S.; Hargreaves, R.J.; Hashemi, R.; Karlovets, E.V.; Skinner, F.M.; Conway, E.K.; Hill, C.; Kochanov, R.V.; Tan, Y.; et al. The HITRAN2020 Molecular Spectroscopic Database. *J. Quant. Spectrosc. Radiat. Transf.* **2022**, *277*, 107949. [CrossRef]
26. Robinson, R.A.; Gardiner, T.D.; Innocenti, F.; Finlayson, A.; Woods, P.T.; Few, J.F.M. First Measurements of a Carbon Dioxide Plume from an Industrial Source Using a Ground Based Mobile Differential Absorption Lidar. *Environ. Sci. Process. Impacts* **2014**, *16*, 1957–1966. [CrossRef] [PubMed]

27. Aiuppa, A.; Fiorani, L.; Santoro, S.; Parracino, S.; D'Aleo, R.; Liuzzo, M.; Maio, G.; Nuvoli, M. New Advances in Dial-Lidar-Based Remote Sensing of the Volcanic CO_2 Flux. *Front. Earth Sci.* **2017**, *5*, 15. [CrossRef]
28. Innocenti, F.; Gardiner, T.; Robinson, R. Uncertainty Assessment of Differential Absorption Lidar Measurements of Industrial Emissions Concentrations. *Remote Sens.* **2022**, *14*, 4291. [CrossRef]

Disclaimer/Publisher's Note: The statements, opinions and data contained in all publications are solely those of the individual author(s) and contributor(s) and not of MDPI and/or the editor(s). MDPI and/or the editor(s) disclaim responsibility for any injury to people or property resulting from any ideas, methods, instructions or products referred to in the content.